

# Clusters of iron-rich cells in the upper beak of pigeons are macrophages not magnetosensitive neurons

Christoph Daniel Treiber<sup>1</sup>, Marion Claudia Salzer<sup>1</sup>, Johannes Riegler<sup>2</sup>, Nathaniel Edelman<sup>1</sup>, Cristina Sugar<sup>1</sup>, Martin Breuss<sup>1</sup>, Paul Pichler<sup>1</sup>, Herve Cadiou<sup>3</sup>, Martin Saunders<sup>4</sup>, Mark Lythgoe<sup>2</sup>, Jeremy Shaw<sup>4</sup> & David Anthony Keays<sup>1</sup>

Understanding the molecular and cellular mechanisms that mediate magnetosensation in vertebrates is a formidable scientific problem<sup>1,2</sup>. One hypothesis is that magnetic information is transduced into neuronal impulses by using a magnetite-based magnetoreceptor<sup>3,4</sup>. Previous studies claim to have identified a magnetic sense system in the pigeon, common to avian species, which consists of magnetite-containing trigeminal afferents located at six specific loci in the rostral subepidermis of the beak<sup>5–8</sup>. These studies have been widely accepted in the field and heavily relied upon by both behavioural biologists and physicists<sup>9–11</sup>. Here we show that clusters of iron-rich cells in the rostral-medial upper beak of the pigeon *Columbia livia* are macrophages, not magnetosensitive neurons. Our systematic characterization of the pigeon upper beak identified iron-rich cells in the stratum laxum of the subepidermis, the basal region of the respiratory epithelium and the apex of feather follicles. Using a three-dimensional blueprint of the pigeon beak created by magnetic resonance imaging and computed tomography, we mapped the location of iron-rich cells, revealing unexpected variation in their distribution and number—an observation that is inconsistent with a role in magnetic sensation. Ultrastructure analysis of these cells, which are not unique to the beak, showed that their subcellular architecture includes ferritin-like granules, siderosomes, haemosiderin and filopodia, characteristics of iron-rich macrophages. Our conclusion that these cells are macrophages and not magnetosensitive neurons is supported by immunohistological studies showing co-localization with the antigen-presenting molecule major histocompatibility complex class II. Our work necessitates a renewed search for the true magnetite-dependent magnetoreceptor in birds.

Each year millions of birds complete lengthy journeys guided by the Earth's magnetic field. Current evidence indicates that the detection of magnetic fields is mediated by an inclination-sensitive light-dependent compass that resides in the retina<sup>12,13</sup>, and an intensity-sensitive apparatus that is believed to provide information about the magnetic map, is associated with the trigeminal nerve, and is thought to rely on biogenic magnetite (Fe<sub>3</sub>O<sub>4</sub>)<sup>14</sup>. The trigeminal nerve was first implicated in magnetoreception in the bobolink *Dolichonyx oryzivorus*, and was suggested to be sensitive to small alterations in magnetic stimuli<sup>15</sup>. Subsequent studies revealed that the ophthalmic branch is required for pigeons to perform an intensity-based conditioning task<sup>3</sup>, and that neurons in the trigeminal brainstem complex of European robins are activated when the birds are subjected to non-uniform magnetic fields<sup>16</sup>. These data have led to the proposition that the sensory cells responsible for magnetite-based magnetoreception lie in the upper beak of birds<sup>3,17</sup>. Previous studies<sup>5,7</sup> have claimed that clusters of iron-containing neurons in six specific bilateral locations in the rostral dermis of the upper beak of pigeons constitute a magnetic sense system<sup>7</sup>. It has been contended that this system consists of unmyelinated dendrites that contain superparamagnetic spherules surrounded by iron platelets that are composed of magnetite and

maghemite, and that the system is a common sensory apparatus in birds<sup>5–7</sup>. These assertions have formed the basis for a host of behavioural studies and theoretical calculations that aim to advance the magnetite theory of magnetoreception<sup>9,10,18–20</sup>.

To investigate this putative magnetic sense system, we undertook a systematic analysis of the prevalence and distribution of all iron-rich cells in the upper beak of the pigeon. We perfused adult pigeons (Nuremberg cohort,  $n = 12$ ), and sectioned the upper beak from the caudal respiratory concha to the tip of the beak in the coronal plane (Fig. 1a, b). We stained serial sections (10  $\mu\text{m}$ ) with Prussian blue (PB) to label ferric iron, and nuclear fast red (NFR) to identify nuclei, followed by counting of all PB-positive cells. We consistently observed PB-positive cells in three specific regions: (1) in the stratum laxum of the dorsal and/or ventral subepidermis; (2) in the buds of feather follicles; and (3) in the basal region of the respiratory epithelium (Fig. 1c–e). We confirmed this pattern of staining in a larger collection of pigeons originating from seven different lofts ( $n = 172$ ). PB-positive cells in all three regions were characterized by the presence of multiple dark blue spherules (0.25–5.0  $\mu\text{m}$  in size) and/or by light blue cytoplasmic staining with a notable nucleus (Fig. 1g–k and Supplementary Figs 1–3). Subepidermal PB-positive cells in caudal and medial regions were predominantly found in the dorsal subepidermis (Fig. 1c), whereas those PB-positive cells located rostrally were found in the ventral subepidermis lining the inner roof of the beak (Fig. 1f and Supplementary Fig. 1). PB-positive cells in the feather follicle clustered in the apical region of the bud (Fig. 1d and Supplementary Fig. 2), and those in the respiratory epithelium were predominantly found within the lateral edges of the concha (Fig. 1e and Supplementary Fig. 3).

As it is believed that iron-rich cells in the upper pigeon beak are limited to six discrete bilateral anatomical loci<sup>5</sup>, we mapped the distribution of PB-positive cells along the rostro-caudal axis of the beak. To do this accurately we first created a three-dimensional topographic map of the pigeon beak by undertaking high-resolution magnetic resonance imaging (MRI) coupled with micro-computed tomography (micro-CT) scanning, identifying four specific anatomical landmarks (Supplementary Movies 1, 2 and Supplementary Figs 4, 5). After staining serial sections, we counted PB-positive cells and used our landmarks to map the distribution of cells along the rostro-caudal axis ( $n = 12$ ). We found that PB-positive cells in the respiratory epithelium and feather follicles were restricted to caudal regions, whereas those in the subepidermal region were found in clusters along the length of the beak with no apparent bilateralization (Fig. 2a–c and Supplementary Figs 6, 7 and Supplementary Table 1). We found no significant differences in the total number of PB-positive cells between sexes (respiratory epithelium ( $P > 0.5$ ), subepidermis ( $P > 0.1$ ), feather follicle ( $P > 0.1$ )) (Supplementary Fig. 8), but observed an extremely large variation in the number and distribution of PB-positive cells when comparing birds of the same age and sex. For instance, pigeon 200 had ~200 PB-positive cells in the subepidermis, whereas pigeon

<sup>1</sup>Institute of Molecular Pathology, Dr Bohr-Gasse, 1030 Vienna, Austria. <sup>2</sup>Centre for Advanced Biomedical Imaging (CABI), Department of Medicine and Institute of Child Health, University College London (UCL), London WC1E 6DD, UK. <sup>3</sup>Université de Strasbourg, Institut des Neurosciences Cellulaires et Intégratives (INCI), CNRS UPR 3212, F-67084 Strasbourg, France. <sup>4</sup>Centre for Microscopy, Characterisation and Analysis, The University of Western Australia, Crawley 6009, Australia.

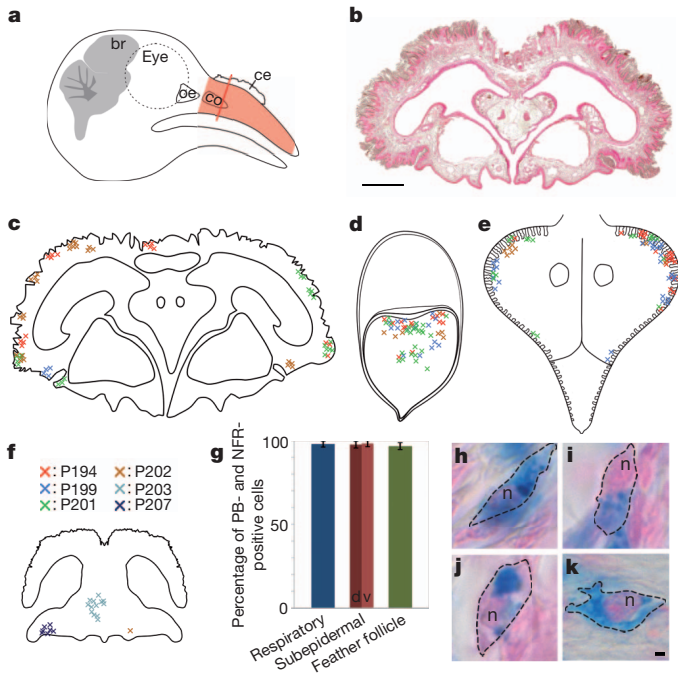


**Figure 1 | PB-positive cells in the upper beak.** **a**, Schematic showing the head of an adult pigeon. The area shaded red indicates the region of the beak that was sectioned, stained and screened for PB-positive cells. br, brain; ce, cere; co, concha; oe, olfactory epithelium. **b**, Upper beak coronal section stained with PB and NFR (the rostro-caudal location of the section is indicated with a red line in **a**). Scale bar, 2 mm. **c**, Schematic of a coronal section highlighting the non-uniform distribution of PB-positive cells in the subepidermal region in four different birds. **d**, **e**, Schematic of a feather follicle and concha showing the location of PB-positive cells in four birds. **f**, Schematic of a coronal section rostral to the cere, showing the non-uniform distribution of PB-positive cells in the subepidermis in three different birds. **g**, Quantification of NFR staining in PB-positive cells revealing that at least 97% of cells in all regions are nucleated ( $n \geq 5$  birds,  $n \geq 180$  cells), **d**, dorsal; **v**, ventral. Error bars show the standard deviation. **h–k**, Representative PB-positive cells in which the nuclei are visible (cell membranes are highlighted by a dashed line, nuclei are marked with n). See also Supplementary Figs 1–3. Scale bar, 1  $\mu$ m.

203 had  $\sim 108,800$  PB-positive cells located in numerous clusters along the length of the beak. Although our serial quantification samples a section every 120  $\mu$ m we did not find the six 350- $\mu$ m-long bilateral clusters that are claimed to constitute a magnetic sense system<sup>7</sup>. We speculated that our pigeon strain might harbour a large genomic deletion that accounts for the absence of this putative magnetosensitive system. To investigate this we quantified PB-positive cells in pigeons from another loft (Vienna cohort,  $n = 6$ ). Similar to our Nuremberg cohort we did not find six bilateral clusters, and once again observed a large variation in the distribution and number of PB-positive cells (Supplementary Fig. 9 and Supplementary Table 2). This variation is not consistent with a genetically encoded sensory apparatus responsible for magnetosensation.

Next we asked whether PB-positive cells are neurons by triple staining sections with PB, NFR, and one of three different antibodies that label neuronal structures: neurofilament (NF), TUBB3 and MAP1B ( $n \geq 5$  birds). In the respiratory epithelium we observed 0.04% co-localization with NF ( $n = 1,208$  cells), 0.6% co-localization with TUBB3 ( $n = 2,818$  cells), and 0.01% co-localization with MAP1B ( $n = 2,213$  cells). In the subepidermis we found no co-localization with NF ( $n = 471$  cells) or MAP1B ( $n = 803$  cells), and only 0.06% co-localization with TUBB3 ( $n = 1,309$  cells). Finally, in the feather follicle we found no co-localization with NF ( $n = 286$  cells) or MAP1B ( $n = 295$  cells), and only 0.24% co-localization with TUBB3 ( $n = 407$  cells) (Supplementary Figs 10, 11). The simplest explanation for the

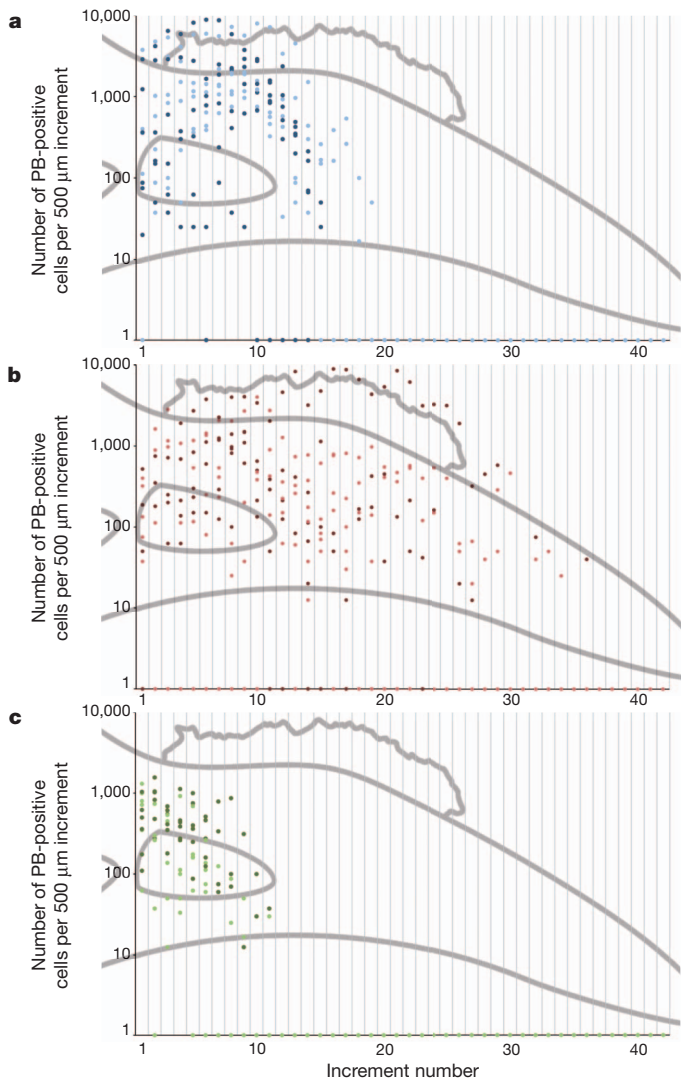


**Figure 2 | Number and distribution of PB-positive cells in the upper beak.** **a–c**, Plots showing the number of PB-positive cells per 500  $\mu$ m increment along the length of the beak in the respiratory epithelium (**a**) (blue dots), subepidermis (**b**) (red dots) and the feather follicle (**c**) (green dots) ( $n = 12$  birds). Each dot represents the number of PB-positive cells in an individual bird in that increment, with males ( $n = 6$ ) shown in dark colours and females ( $n = 6$ ) in light colours. PB-positive cells in the feather follicle and respiratory epithelium are predominantly found in caudal regions, whereas cells in the subepidermis are found along the length of the beak but are most prevalent beneath the cere. Total cell numbers per increment are plotted on a logarithmic axis, highlighting the large variation between birds. Individual birds are shown in Supplementary Figs 6 and 7.

very small amount of apparent co-localization we observed is that two cells, one PB positive and the other positive for a neuronal marker, lie in the same vertical plane, and because of the nature of the chemical stain used cannot be distinguished from one another. Taken together, our results strongly suggest that the clusters of PB-positive cells in the beak of the pigeon are not neurons.

To ascertain the true identity of the PB-positive cells, we undertook an analysis of their ultrastructure using transmission electron microscopy (TEM) ( $n = 3$  birds) (Supplementary Fig. 12). We observed ferritin-like granules (6–9 nm) throughout the cytoplasm of PB-positive cells from all regions and in some instances haemosiderin masses and/or membrane-bound electron-dense organelles known as siderosomes<sup>21,22</sup> ( $\sim 300$  nm) (Fig. 3a–f and Supplementary Fig. 13). Energy-filtered transmission electron microscopy (EFTEM) confirmed that each electron-dense granule was composed of iron (Supplementary

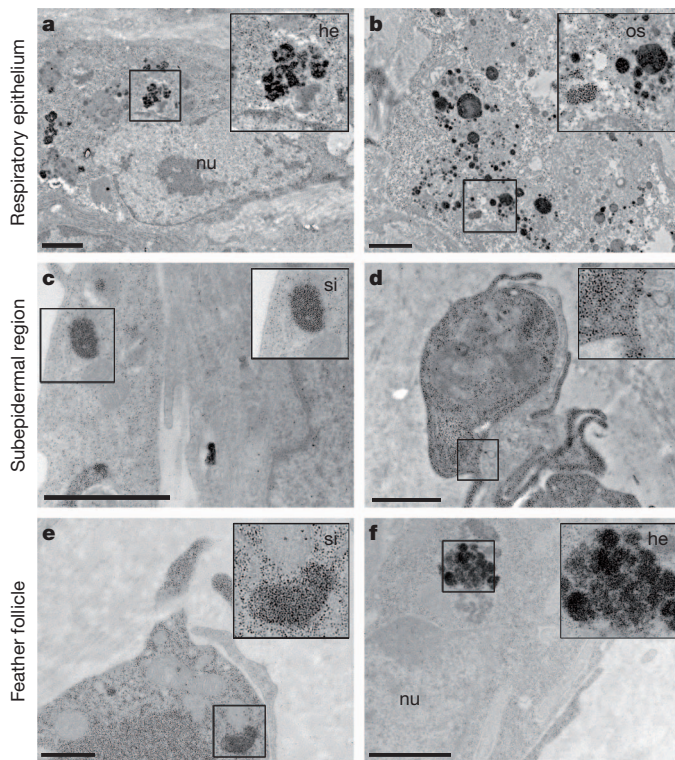


**Figure 3 | Ultrastructure of PB-positive cells.** a–f, Representative electron micrographs of two different PB-positive cells in the respiratory epithelium (a, b), subepidermal region (c, d) and the feather follicle (e, f;  $n = 3$  birds). Cells in all regions were found to contain ferritin-like granules (6–9 nm in diameter) that are present throughout the cytoplasm. In addition we observed haemosiderin (he) clumps and/or membrane bound siderosomes (si). Osmophilic lipid droplets (os) are visible in cells in the respiratory epithelium in b. Cells in the subepidermal region and feather follicle were noted for their slender cytoplasmic projections resembling filopodia, that are seen to engulf a cell in d. Cells in all regions were nucleated (nu). See also Supplementary Fig. 13. Scale bars, 1  $\mu$ m.

Fig. 14). Selected area electron diffraction (SAED) failed to identify any cellular structures that contained magnetite, but showed that haemosiderin masses in the feather follicle consist of a goethite-like material ( $n = 3$  birds), whereas siderosomes in the respiratory epithelium are comprised of ferrihydrite ( $n = 2$  birds) (Supplementary Fig. 15 and Supplementary Table 3). On a cellular level, PB-positive cells in the respiratory epithelium are characterized by the presence of osmophilic lipid vacuoles (Fig. 3b), whereas those cells originating from the feather follicle and subepidermal region had notable dendritic extensions that resembled filopodia (Supplementary Fig. 13d–i, k). In some instances these cytoplasmic tentacles appeared to engulf neighbouring cells, suggesting to us that the PB cells may be phagocytic macrophages (Fig. 3d).

Macrophages are known to reside in the spleen, dermis and respiratory mucosa of multiple species, and to have a vital role in host defence and iron homeostasis<sup>23</sup>. Iron accumulates within macrophages during the catabolism of haemoglobin and is stored as ferritin<sup>24</sup>. In one class of macrophages known as siderophages, ferritin accumulates in membrane-bound siderosomes, which can then undergo proteolytic processing forming haemosiderin. This accumulation of iron renders these cells PB positive<sup>25,26</sup>. To ascertain whether the PB-positive cells in the upper beak of the pigeon were siderophages, we stained cryosections with sera against major histocompatibility complex class II (MHC II), which labels antigen-presenting cells including macrophages, alongside positive and negative controls ( $n \geq 4$  birds) (Fig. 4a–c and Supplementary Fig. 11)<sup>27</sup>. We observed MHC II co-localization with 98.8% of PB-positive cells in the respiratory epithelium ( $n = 104$  cells),

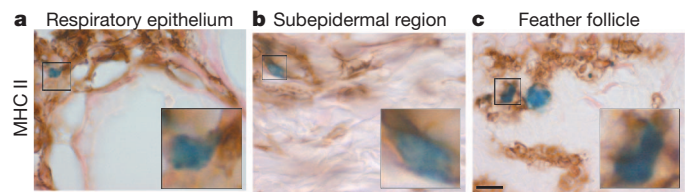


**Figure 4 | MHC II immunohistochemistry on PB-positive cells.**

a–c, Representative images of coronal sections triple stained with PB, NFR, and sera against the antigen-presenting marker MHC II ( $n \geq 4$  birds). MHC II staining was predominant on the surface of cells and found to co-localize with  $\geq 94\%$  of PB-positive cells in all regions. Controls are shown in Supplementary Fig. 11. Scale bar, 10  $\mu$ m.

95% of PB-positive cells in the subepidermis ( $n = 92$  cells), and 94.4% in the feather follicle ( $n = 205$  cells). Taken together with our anatomical mapping, subcellular data and neuronal staining, we conclude that clusters of PB-positive cells in the upper beak of the pigeon *C. livia* are macrophages, not magnetosensitive neurons.

As macrophages are not unique to the upper beak, our finding predicts that PB-positive cells should be found throughout the pigeon. To test this we stained skin samples from the back, abdomen, neck, scalp, wing and lower beak of the pigeon ( $n \geq 3$  birds). This revealed widespread PB-positive staining in the subepidermis and feather follicle, which was indistinguishable from that observed in the upper beak (Supplementary Fig. 16). Our conclusion further predicts the infiltration of PB-positive macrophages in response to tissue damage or host invasion. We observed such a response in the beak of one of our pigeons (P199), where a large inflammatory lesion with a necrotic centre was surrounded by lymphoplasmacytic cells, including  $\sim 80,000$  PB-positive cells that were again characterized by constellations of blue spherules and/or by light blue cytoplasmic staining (Supplementary Fig. 17).

Although we cannot exclude the possibility that a small number of sparsely distributed magnetoreceptors reside at an unknown location in the upper beak of pigeons, this study finds no evidence to support the existence of a subepidermal magnetic sense system that consists of iron-containing dendrites at six specific bilateral loci. This conclusion, which is supported by a critical analysis of the elemental composition of PB-positive cells in the subepidermis<sup>28</sup>, has several important implications. First, it requires a re-evaluation of behavioural studies that have purported to impair the function of a magnetite-based receptor in the subepidermis of the upper beak and the conclusions that these studies reached<sup>9,20</sup>. Second, it necessitates a re-assessment as to whether superparamagnetic magnetite has the necessary physical and magnetic properties to act as a magnetosensor in a living system<sup>10,11,19</sup>. Third, our work reveals that the sensory cells that are responsible for trigeminally mediated magnetic sensation in birds remain undiscovered. These enigmatic cells may reside in the olfactory epithelium, a sensory structure that has been implicated in magnetoreception in the rainbow trout<sup>29</sup>.

## METHODS SUMMARY

**Histological studies.** We perfused adult pigeons with 4% phosphate-buffered paraformaldehyde (PFA, pH 7.4), and dissected the tissue with ceramic-coated tools. We embedded the tissue in paraffin and prepared 10- $\mu$ m coronal sections. We stained sections for 20 min in 5% potassium hexacyanoferrate with 10% HCl, followed by a series of washes and a 2 min exposure to NFR. For immunohistochemistry we incubated the sections with the primary antibody for 18 h in 0.1% Triton PBS with 2–4% milk (pH 7.4), before detection using standard methods, followed by PB staining.

**Ultrastructure studies.** Adult pigeons were perfused with 2.5% glutaraldehyde supplemented with 2% PFA in PBS (pH 7.4). Tissue was dissected with ceramic-coated tools, incubated for 1 h in phosphate-buffered 2% osmium (pH 7.4), dehydrated and embedded in epoxy resin. We prepared alternative semi-thin (2  $\mu$ m) and ultra-thin (70 nm) sections. Semi-thin sections were stained with PB, and the ultra-thin sections were used for TEM, EFTEM and SAED.

**Imaging studies.** Adult pigeons were perfused with 4% PFA. Following post-fixation and mounting, MRI imaging was performed on a horizontal bore 9.4 T DirectDrive VNMRs system (Agilent Technologies), and CT on a Nucline Nano SPECT/CT imaging system (Mediso).

**Full Methods** and any associated references are available in the online version of the paper at [www.nature.com/nature](http://www.nature.com/nature).

**Received 12 December 2011; accepted 19 March 2012.**

**Published online 15 April 2012.**

- Mouritsen, H. & Ritz, T. Magnetoreception and its use in bird navigation. *Curr. Opin. Neurobiol.* **15**, 406–414 (2005).
- Johnsen, S. & Lohmann, K. J. The physics and neurobiology of magnetoreception. *Nature Rev. Neurosci.* **6**, 703–712 (2005).
- Mora, C. V., Davison, M., Wild, J. M. & Walker, M. M. Magnetoreception and its trigeminal mediation in the homing pigeon. *Nature* **432**, 508–511 (2004).
- Kirschvink, J. L., Walker, M. M. & Diebel, C. E. Magnetite-based magnetoreception. *Curr. Opin. Neurobiol.* **11**, 462–467 (2001).
- Fleissner, G. *et al.* Ultrastructural analysis of a putative magnetoreceptor in the beak of homing pigeons. *J. Comp. Neurol.* **458**, 350–360 (2003).
- Falkenberg, G. *et al.* Avian magnetoreception: elaborate iron mineral containing dendrites in the upper beak seem to be a common feature of birds. *PLoS ONE* **5**, e9231 (2010).
- Fleissner, G., Stahl, B., Thalau, P., Falkenberg, G. & Fleissner, G. A novel concept of Fe-mineral-based magnetoreception: histological and physicochemical data from the upper beak of homing pigeons. *Naturwissenschaften* **94**, 631–642 (2007).
- Hanzlik, M. *et al.* Superparamagnetic magnetite in the upper beak tissue of homing pigeons. *Biometals* **13**, 325–331 (2000).
- Wiltshcko, R., Schiffner, I., Fuhrmann, P. & Wiltshcko, W. The role of the magnetite-based receptors in the beak in pigeon homing. *Curr. Biol.* **20**, 1534–1538 (2010).
- Solov'yov, I. A. & Greiner, W. Theoretical analysis of an iron mineral-based magnetoreceptor model in birds. *Biophys. J.* **93**, 1493–1509 (2007).
- Davila, A. F., Winklhofer, M., Shcherbakov, V. P. & Petersen, N. Magnetic pulse affects a putative magnetoreceptor mechanism. *Biophys. J.* **89**, 56–63 (2005).
- Zapka, M. *et al.* Visual but not trigeminal mediation of magnetic compass information in a migratory bird. *Nature* **461**, 1274–1277 (2009).
- Ritz, T., Thalau, P., Phillips, J. B., Wiltshcko, R. & Wiltshcko, W. Resonance effects indicate a radical-pair mechanism for avian magnetic compass. *Nature* **429**, 177–180 (2004).
- Cadiou, H. & McNaughton, P. A. Avian magnetite-based magnetoreception: a physiologist's perspective. *J. R. Soc. Interface* **7** (suppl. 2), S193–S205 (2010).
- Beason, R. C. & Semm, P. Magnetic responses of the trigeminal nerve system of the bobolink (*Dolichonyx oryzivorus*). *Neurosci. Lett.* **80**, 229–234 (1987).
- Heyers, D., Zapka, M., Hoffmeister, M., Wild, J. M. & Mouritsen, H. Magnetic field changes activate the trigeminal brainstem complex in a migratory bird. *Proc. Natl Acad. Sci. USA* **107**, 9394–9399 (2010).
- Williams, M. N. & Wild, J. M. Trigeminal innervated iron-containing structures in the beak of homing pigeons, and other birds. *Brain Res.* **889**, 243–246 (2001).
- Wiltshcko, W., Munro, U., Ford, H. & Wiltshcko, R. Avian orientation: the pulse effect is mediated by the magnetite receptors in the upper beak. *Proc. Biol. Sci.* **276**, 2227–2232 (2009).
- Solov'yov, I. A. & Greiner, W. Micromagnetic insight into a magnetoreceptor in birds: existence of magnetic field amplifiers in the beak. *Phys. Rev. E* **80**, 041919 (2009).
- Stapput, K., Thalau, P., Wiltshcko, R. & Wiltshcko, W. Orientation of birds in total darkness. *Curr. Biol.* **18**, 602–606 (2008).
- Iancu, T. C. Ferritin and hemosiderin in pathological tissues. *Electron Microsc. Rev.* **5**, 209–229 (1992).
- Richter, G. W. The iron-loaded cell—the cytopathology of iron storage. A review. *Am. J. Pathol.* **91**, 362–404 (1978).
- Wang, J. & Pantopoulos, K. Regulation of cellular iron metabolism. *Biochem. J.* **434**, 365–381 (2011).
- Mebius, R. E. & Kraal, G. Structure and function of the spleen. *Nature Rev. Immunol.* **5**, 606–616 (2005).
- Meguro, R. *et al.* The presence of ferric and ferrous iron in the nonheme iron store of resident macrophages in different tissues and organs: histochemical demonstrations by the perfusion-Perls and -Turnbull methods in the rat. *Arch. Histol. Cytol.* **68**, 171–183 (2005).
- Simson, J. V. & Spicer, S. S. Ferritin particles in macrophages and in associated mast cells. *J. Cell Biol.* **52**, 536–541 (1972).
- Igyártó, B. Z., Lacko, E., Olah, I. & Magyar, A. Characterization of chicken epidermal dendritic cells. *Immunology* **119**, 278–288 (2006).
- Winklhofer, M. & Kirschvink, J. Does avian magnetoreception rely on both magnetite and maghemite? <http://arxiv.org/abs/0805.2249> (2008).
- Walker, M. M. *et al.* Structure and function of the vertebrate magnetic sense. *Nature* **390**, 371–376 (1997).

**Supplementary Information** is linked to the online version of the paper at [www.nature.com/nature](http://www.nature.com/nature).

**Acknowledgements** We would like to thank M. Busslinger, M. Wild and J. Flint for their critical comments on earlier drafts of this manuscript. Thanks also to T. Iancu who commented on our electron micrographs and S. Soto who remarked on the inflammatory lesion in P199. Gratitude is owed to the bio-optics and electron microscopy facilities at the Institute of Molecular Pathology for their assistance in performing experiments. We wish to acknowledge the Centre for Microscopy, Characterisation and Analysis and the Australian Microscopy and Microanalysis Research Facility at the University of Western Australia, a facility funded by the University, State and Commonwealth Governments. Finally, we wish to thank Boehringer Ingelheim, which funds basic science at the Institute of Molecular Pathology.

**Author Contributions** D.A.K. and C.D.T. conceived and designed the study. M.C.S., C.D.T., M.B., P.P., C.S. and N.E., performed the sectioning, PB staining and counting. D.A.K., C.D.T. and H.C. analysed the resultant data. J.R. and M.L. performed the MRI and CT studies, producing the three-dimensional structure of the pigeon beak. D.A.K. performed the immunohistochemical studies. C.D.T. performed the ultrastructure experiments and J.S. and M.S. did the EFTEM and SAED studies and analysed the data. D.A.K. wrote the paper, and all authors commented on the manuscript.

**Author Information** Reprints and permissions information is available at [www.nature.com/reprints](http://www.nature.com/reprints). The authors declare no competing financial interests. Readers are welcome to comment on the online version of this article at [www.nature.com/nature](http://www.nature.com/nature). Correspondence and requests for materials should be addressed to D.A.K. ([keays@imp.ac.at](mailto:keays@imp.ac.at)).

## METHODS

**PB staining.** We optimized our PB-staining protocol on our large cohort of pigeons ( $n = 172$ ) that we sourced from seven different lofts. We experimented with a variety of different fixatives, section thickness, and blades before adopting the following protocol. Adult homing pigeons ( $n = 12$  Nuremberg cohort,  $n = 6$  Vienna cohort) were killed before perfusion with 4% phosphate-buffered paraformaldehyde (PFA, pH 7.4). The tissue was dissected with ceramic-coated tools and post-fixed for 18 h before dehydration in an increasing alcohol series. The tissue was then embedded in paraffin and sectioned coronally (10  $\mu\text{m}$ ) with ceramic-coated microtome blades (DuraEdgeHigh Profile, BLM00103P). Four consecutive coronal sections were mounted on positively charged microscope slides (Menzel Superfrost PLUS, Thermo Scientific). For PB staining we incubated every third slide in a freshly prepared solution of 5% potassium hexacyanoferrate (Sigma, P9387) in 10% HCl for 20 min. After three washes in double distilled  $\text{H}_2\text{O}$ , sections were counterstained for 2 min in NFR (Sigma, 60700). Each slide was then scanned (MIRAX Slide Scanner) and PB-positive cells counted manually, using light microscopy where necessary. For anatomical mapping, landmarks were identified (Supplementary Fig. 5), and 500- $\mu\text{m}$ -thick increments determined. To obtain estimated total cell counts the number of PB-positive cells counted within a normalized increment were divided by the number of sections counted within that increment and multiplied by a factor of 50 (see Supplementary Tables 1 and 2). We compared the number of PB-positive cells in males and females by performing a Student's *t*-test. All pigeons were sexed using genetic methods as previously described<sup>30</sup>, and experiments were performed in accordance with the relevant guidelines and regulations (Magistrat 60, Veterinäramt, MA60-001603/2010/002).

**Immunohistochemistry.** For staining with neuronal antibodies slides were deparaffinized and washed in PBS (pH 7.4) before incubation with the primary antibody for 18 h in 0.1% Triton PBS with 2% milk (pH 7.4). Primary antibodies were used at the following concentrations: NF (Millipore, MAB1621, 1:2,000), TUBB3 (Covance, MMS-435P, 1:1,000), MAP1B (Santa Cruz, SC-58784, 1:75). Following a series of washes in PBS, slides were incubated for 2 h with a biotinylated secondary antibody (1:500), before visualization with a peroxidase-based Vectastain Elite ABC kit (Vector Labs, PK-4002) and the chromophore DAB (3,5-diaminobenzidine, Dako). For MHCII staining, 10- $\mu\text{m}$  cryosections were prepared, quenched in 2%  $\text{H}_2\text{O}_2$  in PBS for 30 min, before incubation for 18 h in 0.1% Triton PBS with 4% milk (pH 7.4) with the primary antibody (Santa Cruz, SC-59323, 1:500). This antibody is a mouse monoclonal antibody raised against white blood cells originating from the chicken. To avoid cross reaction with endogenous biotin/avidin, a HRP-conjugated secondary antibody was used (Biorad, 1:500), and staining visualized with DAB. Sections were thoroughly washed with PBS before PB staining and scanning as described above. All cell counting and co-localization studies were performed blinded to the antibody used. The overall percentage of co-localization was determined by calculating the rate of co-localization per bird, and ascertaining the mean.

**Ultrastructure studies.** Adult pigeons were perfused with 2.5% glutaraldehyde supplemented with 2% PFA in PBS (pH 7.4) (Glut-PFA), before tissue dissection with ceramic-coated tools. Following post-fixation for 48 h, this tissue was washed with PBS, incubated for 1 h in phosphate-buffered 2% osmium (pH 7.4), dehydrated and embedded in epoxy resin. After polymerization, the blocks were trimmed and sectioned, alternatively taking semi-thin (2  $\mu\text{m}$ ) and ultra-thin (70 nm) sections. The ultra-thin sections were mounted on formvar-film copper slot grids for TEM, whereas the semi-thin sections were etched with 21% sodium ethoxide in ethanol, rehydrated and stained with PB and NFR. Where necessary, PB staining was intensified by incubating the sections in 0.5% DAB<sup>31</sup>. TEM imaging on ultra-thin sections used a 100 kV electron microscope (FEI Morgagni 268D) with a CCD camera (Morada Olympus-SIS). For EFTEM imaging and selected area electron diffraction, the ultra-thin sections were mounted on holey carbon-film copper finder grids (Quantifoil, R3.5/1) and analysed on a 200 kV TEM (JEOL, 2100) fitted with a Gatan Imaging Filter (Tridiem) and CCD camera (Orion SC1000). For EFTEM, bright-field images were taken before obtaining elemental maps for iron, which were acquired using the iron M-edge and generated using the conventional three-window method. Two pre-edge (background) images were acquired at energies of 45 and 50 eV, and the post-edge (signal energy) image was acquired by centring the filter's energy-selecting slit at 59 eV with a slit width of 5 eV (~10 s acquisition time). Diffraction data was obtained from iron deposits identified by EFTEM and the data calibrated against a polycrystalline gold standard.

**MRI.** Animals were killed and perfused with 4% PFA as described above. Following 18 h of post-fixation, heads were mounted in a 70-mm diameter PE tube filled with proton-free perfluoro-polyether fomblin (Solvay Solexis S.p.A.). Imaging was performed on a horizontal bore 9.4 T DirectDrive VNMRS system (Agilent Technologies) using a 72 mm quadrature birdcage volume coil (RAPID Biomedical GmbH). For three-dimensional imaging, a gradient-echo sequence with the following parameters was used: time to echo (TE), 2.8 ms; time to repetition (TR), 280 ms; flip angle, 40°; six averages, field of view, 70  $\times$  70  $\times$  35 mm; matrix size, 512  $\times$  512  $\times$  256. For higher-resolution images of the beak, PFA-fixed beaks were incubated with 8 mM gadolinium solution (Magnevist, Bayer AG) in PBS for 48 h followed by embedding in agar containing 8 mM gadolinium. Gradient-echo images were acquired using the following parameters: TE, 2.7 ms; TR, 25 ms; flip angle, 45°; five averages; field of view, 28  $\times$  28  $\times$  35 mm; matrix size, 560  $\times$  560  $\times$  700. Regions of interest were segmented using thresholds with manual adjustments where necessary using Amira visualization software (v.5.2.2, Visage Imaging).

**CT imaging.** CT imaging was performed on a Nucline Nano SPECT/CT imaging system (Mediso) using the following imaging parameters: 360 projection, pitch 0.5, 55 kVp, 145  $\mu\text{A}$  acquired at 45  $\mu\text{m}$  isotropic reconstructed to 50  $\mu\text{m}$  isotropic.

30. Horng, Y. M., Wu, C. P., Wang, Y. C. & Huang, M. C. A novel molecular genetic marker for gender determination of pigeons. *Theriogenology* **65**, 1759–1768 (2006).
31. Moos, T. & Mollgard, K. A sensitive post-DAB enhancement technique for demonstration of iron in the central nervous system. *Histochemistry* **99**, 471–475 (1993).